

Nanocrystal/Metal-Organic Framework Hybrids as Electrocatalytic Platforms for CO₂ Conversion

Yannick T. Guntern,^[a] James R. Pankhurst,^[a] Jan Vávra,^[a] Mounir Mensi,^[b] Valeria Mantella,^[a] Pascal Schouwink,^[b] and Raffaella Buonsanti^{*[a]}

Abstract: The tunable chemistry linked to the organic/inorganic components in colloidal nanocrystals (NCs) and metal-organic frameworks (MOFs) offers a rich playground to advance the fundamental understanding of materials design for various applications. Here, we combine these two classes of materials by synthesizing NC/MOF hybrids wherein Ag NCs are in intimate contact with Al-PMOF ([Al₂(OH)₂(TCPP)], TCPP = tetrakis(4-carboxyphenyl)porphyrin), to form Ag@Al-PMOF. In our hybrids, the NCs are embedded in the MOF while still preserving electrical contact with a conductive substrate. This key feature allows to explore Ag@Al-PMOF as electrocatalysts for the CO₂ reduction reaction (CO₂RR). We show that the pristine interface between the NCs and the MOFs accounts for electronic changes in the Ag, which suppress the hydrogen evolution reaction (HER) and promote the CO₂RR. We also demonstrate a minor contribution of mass transfer effects imposed by the porous MOF layer under the chosen testing conditions. Furthermore, we find an increased morphological stability of the Ag NCs when combined with the Al-PMOF. The synthesis method is general and applicable to other metal NCs, thus revealing a new way to think about rationally tailored electrocatalytic materials to steer selectivity and improve stability.

Introduction

Chemical transformations often require the catalytic material to possess multiple functionalities in order to be efficient and selective. This concept applies both to homogeneous catalysts, where tunability is achieved by changing the metal center and the organic ligands, and to heterogeneous catalysts, where one of the classical approaches is to tune the metal/support interactions.

Due to its potential of closing the carbon cycle whilst simultaneously storing renewable energy, the electrochemical CO₂ reduction reaction (CO₂RR) is becoming an increasingly important and studied process.^[1,2] Two main problems that persist are: 1) the competition between CO₂RR and the hydrogen evolution reaction (HER) and 2) the poor selectivity amongst the CO₂RR products that are formed. Metallic electrocatalysts are certainly the most investigated systems so far.^[3] However, it is clear that we need to move away from single-component

materials in order to tackle the CO₂RR challenge and to decouple the various parameters impacting CO₂RR selectivity (i.e. geometric and electronic effects, local pH, electrolyte effects).^[4–6] Concrete rules of design for new catalytic materials are yet to be discovered and, due to the complicated CO₂RR reaction pathway, theorists need input from the experimentalists regarding the descriptors which determine selectivity.

Here, we create a novel material platform to explore the chemistry of CO₂RR by combining two of the most tunable and versatile artificial materials, namely colloidal nanocrystals (NCs) and metal-organic frameworks (MOFs).

During recent years, a significant number of studies have shown that MOFs can be utilized as electrocatalysts for CO₂ reduction with the function of support for molecular-type catalysts.^[7–15]

While mainly CO has been obtained as the reduction product, due to the nature of their catalytically active centers, these reports have opened up a new avenue for MOFs. A few attempts were made towards exploring the idea of combining nanostructured metals with MOFs as electrocatalysts for CO₂RR. In one example, Cu@NU-1000 hybrids (where “@” indicates NCs embedded in the MOF) were obtained by performing electrochemical reduction of Cu(II) to Cu(0) directly within the zirconium MOF (NU-1000) film.^[16] While proving that these hybrids are electrocatalytically active, the synthetic approach used here is limited to producing small Cu NCs (<10 nm), which are known to be more selective for HER over CO₂RR. In a second example, gold nanostructured microelectrodes were covered with various MOFs (i.e. ZIF-8, Cu(bdc), Al-PMOF) using layer-by-layer and solvothermal methods.^[17] The resulting films were non uniform and they produced mostly hydrogen. Studies on NC/MOF hybrids for a variety of organic and photocatalytic reactions have demonstrated the importance of precisely controlling and tuning their structure and morphology to achieve catalytic activity and to understand the rules that govern it.^[18–28] This previous literature suggests that more sophisticated synthetic techniques to tune conductive films of NC/MOF hybrids are needed to reveal new paradigms in CO₂RR.

In this work, we synthesize Ag@Al-PMOF hybrid thin films by combining colloidal chemistry, atomic layer deposition (ALD) and solvothermal chemical conversion. We then study their electrocatalytic behavior in CO₂RR and find a more-than-double increase in the selectivity towards CO and a drastic decrease of HER compared to the bare Ag NCs. As a result of the synthetic tunability, we reveal the key role of the pristine Ag/Al-PMOF interface in facilitating electron transfer from the MOF to the NCs which accounts for the enhanced catalytic performance together with minor mass transport effects imposed by the porous MOF layer under the chosen testing conditions. Furthermore, the MOF matrix contributes to improve the morphological stability of the Ag NCs under CO₂RR conditions. The unique performance of the present hybrid catalyst compared to previous literature is attributed to the precision and tunable variation applied in their

[a] Y. T. Guntern, Dr. J. R. Pankhurst, J. Vávra, V. Mantella, Prof. Dr. R. Buonsanti
Laboratory of Nanochemistry for Energy (LNCE), Institute of Chemical Sciences and Engineering (ISIC), École Polytechnique Fédérale de Lausanne, CH-1950 Sion, Switzerland.
raffaella.buonsanti@epfl.ch

[b] Dr. M. Mensi, Dr. P. Schouwink
Institute of Chemical Sciences and Engineering (ISIC), École Polytechnique Fédérale de Lausanne, CH-1950 Sion, Switzerland.

Supporting information for this article is given via a link at the end of the document.

RESEARCH ARTICLE

synthetic design. Finally, we demonstrate that the same approach can be extended to other NCs, thereby revealing a new platform to investigate further the potential of these multicomponent catalysts in CO₂RR and eventually other electrochemical reactions and applications.

Results and Discussion

Regarding the choice of the MOF component for our hybrid catalyst, we selected the porphyrinic Al-PMOF ([Al₂(OH)₂(TCPP)], TCPP = tetrakis(4-carboxyphenyl)porphyrin),^[29] which was previously studied and found to be stable under CO₂RR conditions.^[14] As for the metal NC component, Ag is one of the most promising CO₂RR electrocatalysts due to its high selectivity for CO^[30–37] and is therefore a perfect NC counterpart to study the synergistic interactions with the MOF.

The synthesis of the Ag@Al-PMOF hybrids was performed by adapting a procedure previously reported for much larger Ag NCs.^[38] **Figure 1** summarizes the reaction scheme for the hybrids (**Figure 1a**) and the electron microscopy characterization at each step (**Figures 1b–g**). Spherical Ag NCs (**Figures 1b,e**) with an average size of 10.5 ± 1.4 nm were synthesized and deposited by drop-casting on various substrates (silicon, transmission electron microscopy (TEM) grid, glassy carbon). The high-magnification TEM image in **Figure 1b** confirms the multiple-twinned structure

of the NCs as previously reported.^[39] As organic ligands can impact the electrocatalytic properties of colloidal NCs,^[40] a mild ligand stripping was performed by immersing the NC thin films in acetone for 4 h. The significant decrease of the characteristic C–H absorption bands of oleylamine (OLAM)^[41] around 2900 cm⁻¹ in the infrared spectrum (**Figure S1**) confirms that nearly all of the ligands were removed. Furthermore, N₂ and O₂ plasma treatments were attempted in order to remove the ligands, but the Ag NCs completely sintered under these conditions (**Figure S2**). ALD at 50 °C and a deposition rate of ~0.07 nm/cycle (**Figure S3**) was performed to grow a conformal shell of Al₂O₃ on the Ag NCs as a localized Al precursor for the subsequent MOF formation. The TEM image in **Figure 1c** and the high-angle annular dark-field scanning TEM (HAADF-STEM) image with corresponding energy dispersive X-ray spectroscopy (EDX) elemental maps in **Figure 1f** confirm the formation of the Ag@Al₂O₃ core-shell structure.

The Al₂O₃ shell was then converted into Al-PMOF through a reaction with the TCPP linker in a dimethylformamide (DMF)/H₂O solvent mixture in a microwave reactor. The TEM images of the resulting Ag@Al-PMOF hybrids in **Figures 1d** and **g** show that the Ag NCs are completely embedded in a network of plate-like crystallites with a pristine interface between the two components as confirmed by the EDX analysis in **Figure S4**. The majority of the Ag NCs retained their size and shape during the Al₂O₃ deposition and the MOF growth; only a small fraction of the Ag

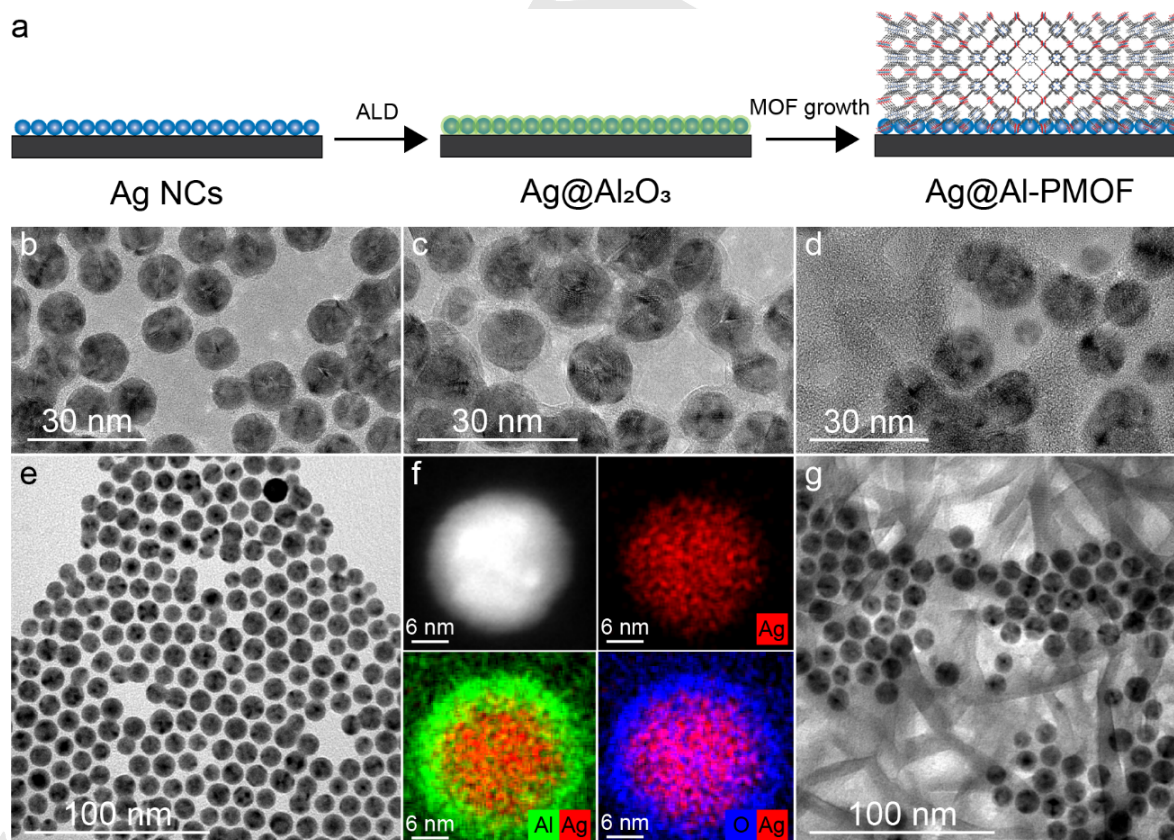


Figure 1. (a) Scheme illustrating the synthesis of Ag@Al-PMOF hybrids. (b–g) TEM characterization of the sample at each step of the synthesis: (b, e) High- and low-magnification TEM images of Ag NCs; (c, f) high-magnification TEM and HAADF-STEM image with corresponding EDX elemental maps for the Ag@Al₂O₃ core-shell particles after 45 ALD cycles; (d, g) high- and low-magnification TEM images of Ag@Al-PMOF hybrids.

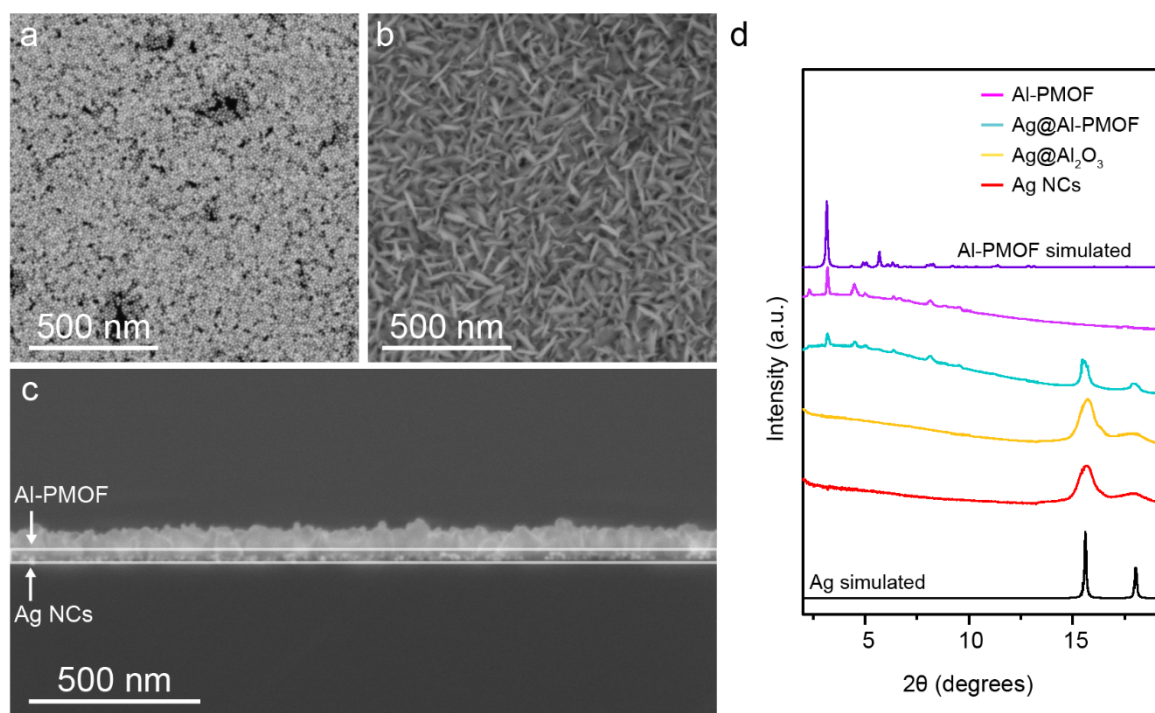


Figure 2. Top-down SEM images of (a) Ag NCs and (b) Ag@Al-PMOF thin films on glassy carbon substrate. (c) Cross-section SEM image of a Ag@Al-PMOF thin film on a Si substrate (from the bottom: Si substrate, Ag NCs, MOF matrix). (d) GIXRD patterns ($\lambda = 0.64066 \text{ \AA}$) of Ag NCs (red), Ag@Al₂O₃ (yellow), Ag@Al-PMOF (cyan) and Al-PMOF (pink) thin films together with the simulated patterns for Ag (black, ICSD-604632) and Al-PMOF (purple, CSD-1500441).

NCs were sintered or etched. To gain insight into the structure and morphology of the hybrid thin films, scanning electron microscopy (SEM) and grazing-incidence X-ray diffraction (GIXRD) were performed (**Figure 2**). The SEM image in **Figure 2a** shows a typical thin film of bare Ag NCs and **Figure 2b** reveals the plate-like MOF crystallites on top of the NCs in the hybrid structure. The contrast difference in the cross-section image (i.e. brighter NCs and darker MOF matrix) in **Figure 2c** shows that a uniform MOF layer with an average thickness of $\sim 50\text{--}80 \text{ nm}$ covers the Ag NCs when converting a $3 \text{ nm Al}_2\text{O}_3$ shell obtained from 45 ALD cycles. Although most of the NCs are completely covered by the MOF and in contact with the conductive substrate, some of them are also detected on top of the MOF crystallites (**Figure S5**). The GIXRD experiments confirmed that the phase and crystallinity of the Ag NCs was retained during the entire synthetic process (**Figure 2d**). Furthermore, the patterns of the Ag@Al-PMOF hybrid and pure MOF thin film both match with the simulated pattern of Al-PMOF. The corresponding 2D detector images (**Figure S6**) as well as the relative peak intensities in the 1D patterns (**Figure 2d**) indicate a preferred orientation of the MOF crystallites as observed in previous work.^[38] Rietveld analysis of the MOF peaks (**Figure S7**) reveals a preferred orientation along the orthorhombic lattice direction [100], which is in agreement with the previously described perpendicular orientation of the porphyrin units relative to the substrate/NC surface.^[38] Moreover, these results indicate that the plate-like morphology of the Al-PMOF crystallites might correlate with the preferred growth direction along the TCPP moieties. To study the chemical interplay between the NCs and the MOF in

our hybrid catalyst, we used an H-type cell filled with CO₂-saturated 0.1 M KHCO_3 electrolyte and flat glassy carbon electrodes as catalyst supports.^[42] Despite the relatively low current densities obtained in this setup, it is more sensitive to changes in the intrinsic activity of the electrocatalysts as opposed to gas diffusion electrodes yielding commercially-viable current densities ($> 200 \text{ mA cm}^{-2}$), which however need to be the next step.^[43]

Figure 3 summarizes the results of the chronoamperometry (CA) experiments performed in the potential range from -0.9 V to -1.4 V vs the reversible hydrogen electrode (RHE), which was selected based on the results of linear-sweep voltammetry (LSV, **Figure S8**). For both the Ag NC and the Ag@Al-PMOF hybrid catalysts, synthesized from 45 ALD cycles, CO and H₂ were detected as gaseous products and formate as the only liquid product (**Figure 3a-c**). Over the entire potential range, the Ag@Al-PMOF exhibits a decreased Faradaic efficiency (FE) for H₂ (**Figure 3a**), while the selectivities for CO and formate increase compared to the bare Ag NCs (**Figures 3b,c**). The highest measured CO selectivity for Ag@Al-PMOF is 55.8 \% ($\pm 2.8 \text{ \%}$) at -1.1 V vs RHE, which corresponds to a 2.2-fold enhancement compared to the Ag NCs. Because the mass loading of Ag NCs is the same among the samples (15 \mu g), the activities of both catalysts are well represented by the as-measured current densities in **Figures 3d-f**. **Figure 3d** shows that the pronounced decrease in the H₂ selectivity for Ag@Al-PMOF is concurrent with the inhibition of the intrinsic catalytic activity for the HER over all measured potentials. On the other hand, the partial current densities for CO and for formate (**Figures 3e and S9**) are very similar between the two

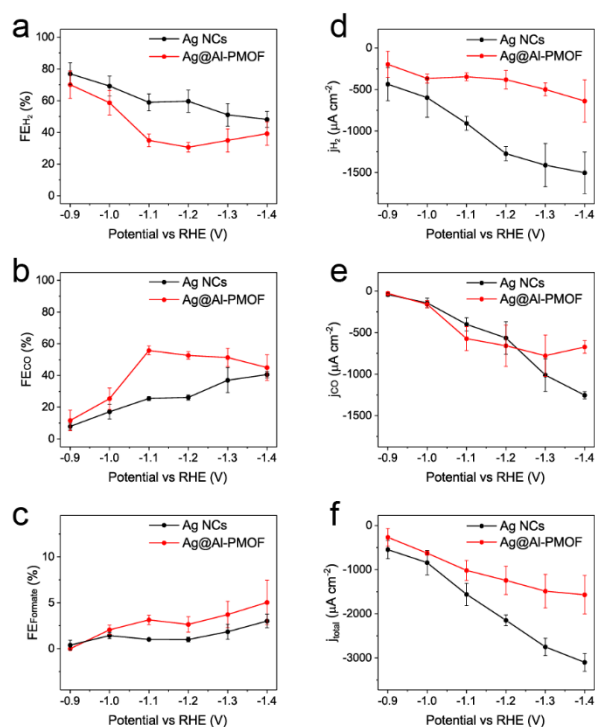


Figure 3. On the left: Faradic efficiencies (FEs) of Ag NCs (black) and Ag@Al-PMOF hybrids synthesized from 45 ALD cycles (red) for (a) H₂, (b) CO and (c) formate as a function of the applied potential. On the right: partial current densities (J) are shown for (d) H₂ and (e) CO, as well as the total current densities (f). Electrocatalytic performance was evaluated in an H-type cell containing CO₂-saturated 0.1 M KHCO₃. The error bars show standard deviations, determined from three independent measurements.

catalysts. A subtle difference is observed at -1.1 V and -1.2 V vs RHE where the reaction towards CO is slightly boosted in the hybrids compared to the bare Ag NCs. As for the total current densities, they are lower in the Ag@Al-PMOF compared with the Ag NCs (**Figure 3f**) and correlate well with the strong inhibition of the HER. A minor contribution to the decreased current might also come from the detachment of a few NCs from the substrate during the preparation of the hybrids (**Figure S5**).

To better understand the electrocatalytic behavior of the hybrids, we prepared a pure MOF thin film and measured its catalytic performance by CA at -1.1 V vs RHE. In agreement with previous work,^[14] the Al-PMOF produced mainly H₂ (**Figure S10**). These results confirm that the HER suppression and the CO production are related to the formation of the hybrid.

Unveiling new mechanisms to promote CO₂RR versus HER is crucial to advancing catalyst design in pH-neutral, additive-free electrolytes. In the Ag@Al-PMOF hybrids several possibilities can be considered to explain the HER suppression and the concomitant CO₂RR promotion, including mass transport limitation imposed by the porous MOF coating and/or changes in the electronic structure of the Ag NCs.

Recently, transport effects within porous electrocatalysts and nanowires have been shown to promote CO₂RR and to inhibit HER due to the increased local pH within the pores.^[44–47] In fact, increased alkalinity slows down the HER rate via local depletion

of proton donors.^[44] Changes in product distribution have also been attributed to variation of the residence time of CO₂ and products within porous copper electrodes.^[48] To verify if the inhibition of HER and concomitant slight promotion of CO₂RR in our hybrid catalyst can be attributed to similar diffusional-gradients of both reactants and products within the MOF pores (pore sizes of 6×11 Å and 5 Å),^[29] we performed different sets of experiments. First of all, we attempted to study diffusion of humid CO₂ across an Al-PMOF membrane, which was prepared following a previous study.^[49] Despite encouraging SEM results showing a uniform crack-free film (**Figure S11**), the presence of intercrystallite gaps and defects impeded us to obtain any insights, which require a dedicated follow-up study. In order to study local pH effects related to transport limitations imposed by the presence of the porous MOF layer, we varied the concentration of the electrolyte and the thickness of the MOF. **Figure 4** compares the FEs of the bare Ag NCs and the Ag@Al-PMOF, synthesized from 15 and 45 ALD cycles, in 0.1 M KHCO₃ and 0.5 M KHCO₃. Going from a thinner to a thicker MOF layer, one expects a more pronounced effect of the mass transport limitation, implying a decrease in HER and an increase in the CO production due to a higher local pH. In fact, this behavior is observed at the higher buffer capacity. Instead, at lower buffer capacity, there is no notable difference in the FEs corresponding to the two thicknesses. This finding suggests that electronic effects should also be considered.

Electronic effects have explained the behavior of NC/MOF hybrids in catalysis as well as in other applications, and X-ray photoelectron spectroscopy (XPS) is so far the most used technique to investigate the interactions between these two domains.^[22,23,50,51] Thus, this technique was utilized to study our hybrids (**Figures 5 and S12**). **Figure 5a** shows that the binding energies of the Ag 3d core levels shift to higher values ($+0.16$ eV) for the Ag NCs embedded in the MOF, which indicates a transfer of electron density from the Al-PMOF to the NCs.^[52,53]

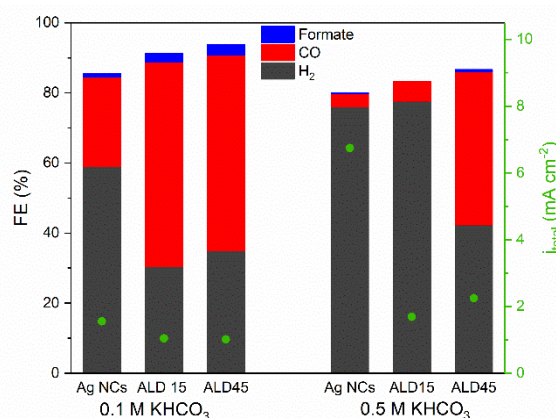


Figure 4. FEs and total current densities for Ag NCs and Ag@Al-PMOF hybrids with different MOF thicknesses, synthesized from 15 or 45 ALD cycles, measured in 0.1 M KHCO₃ and 0.5 M KHCO₃ at -1.1 V vs RHE. We note that the total FE is lower than 100%. Oxidation of some unaccounted formate at the Pt anode has been reported to contribute to the lack of 100% total FE.^[54] Also, some electrons might be driving Ag sintering at higher potential (**Figure 6**), thereby contributing to non-productive current.

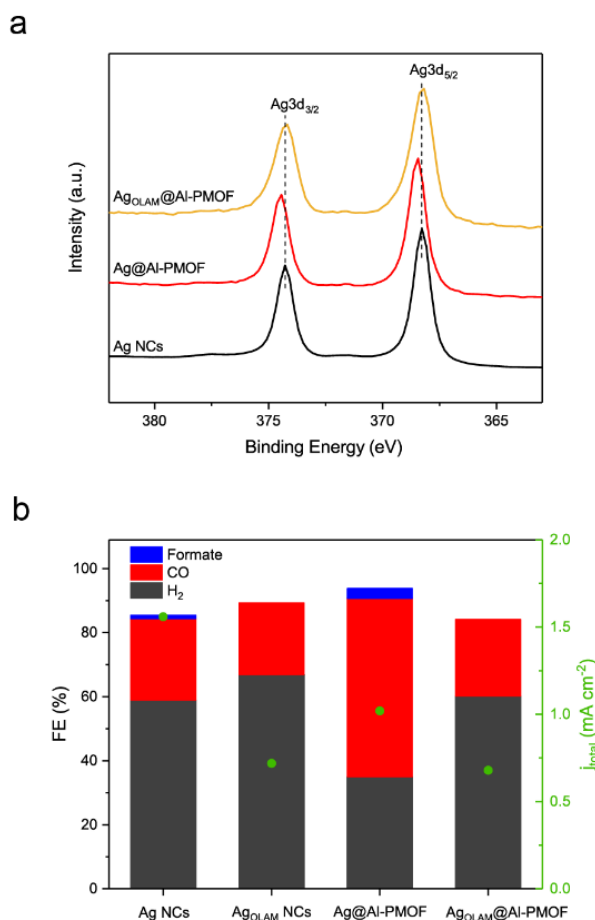


Figure 5. (a) XPS spectra of Ag NCs (black), Ag@Al-PMOF (red) and Ag_{OLAM}@Al-PMOF (yellow). (b) FEs and total current densities for Ag NC and Ag@Al-PMOF catalysts, with and without OLAM ligands, measured at -1.1 V vs RHE.

To confirm the electron enrichment of the Ag within the hybrids, the UV-vis absorption spectra of the Ag NCs and the Ag@Al-PMOF were collected (Figure S13), as the interaction with the MOF should shift the characteristic surface plasmon resonance (SPR) peak of the Ag NCs.^[39] Since the Ag SPR peak is dampened in the hybrid and overlaps with the porphyrin Q bands^[29] from the MOF, it was not possible to reliably discern such a shift. However, the quenching of the photoluminescence (PL) emission of Al-PMOF in the hybrid sample is consistent with an electron transfer from Al-PMOF to the Ag NCs (Figure S14). If charge transfer is occurring between these two domains, one expects the interface between the NC and the MOF to play a significant role. Hence, we synthesized Ag_{OLAM}@Al-PMOF, where the native OLAM ligands were not removed from the surface prior to the growth of the hybrids. For this sample, the Ag3d peaks do not shift compared to the bare Ag NCs (Figure 5a), indicating that the presence of interfacial OLAM ligands prevents the charge transfer in the hybrid. In fact, when tested for CO₂RR (Figure 5b), no significant change in FE and current was observed between the Ag_{OLAM} NCs and the Ag_{OLAM}@Al-PMOF. This result also confirms no impact of the MOF on local pH changes at 0.1 M

KHCO₃ and the higher influence of the electronic effects under these conditions.

Since the nature of the interface seems to play a crucial role for the electron transfer from the MOF to the Ag catalyst, we grew Al-PMOF on a Ag foil and compared its catalytic behavior to that of a bare Ag foil (Figure S15). The Al-PMOF-coated Ag foil was more selective for CO with a decreased FE for H₂; however, the effect was less pronounced compared to the nanostructured Ag@Al-PMOF because of the lower surface-to-volume ratio in the bulk silver foil and hence decreased interfacial area between the MOF and the Ag. Therefore, both interfacial ligands and a decreased interface area lead to a reduced charge transfer from the MOF to the Ag catalyst, impeding the synergistic interaction which improves the catalytic performance.

As a result of the observed electron donation from the MOF to the Ag NCs in the Ag@Al-PMOF, the Ag NCs become electron-rich, which in turn may facilitate the electron transfer to CO₂ as previously observed for other surface-functionalized NC electrocatalysts (i.e. Au NCs with electron-donating N-heterocyclic carbenes as ligands).^[55] The Tafel analysis (Figure S16) reveals a much smaller slope for the Ag@Al-PMOF versus the Ag NCs, which qualitatively indicates an improvement in the rate-limiting single electron transfer to the adsorbed CO₂ on the electron-rich Ag NCs.^[55–57]

With all the above results in mind, the selectivity trends in Figure 3a,b can now be further explained. Here, the FE_{CO} and FE_{H₂} are almost the same for both Ag NCs and the hybrids at -0.9 V vs. RHE, then they diverge as the potential is increased, then they converge again at -1.4 V vs. RHE. Looking at the potential-dependence of the partial current densities (Figure 3d,e), J_{H₂} of the Ag@Al-PMOF is basically flat across the full potential range. Having excluded that mass transfer limitations by the MOF impact the local pH at 0.1 M KHCO₃, this trend must be attributed to electronic effects. Instead, the J_{CO} of the hybrids and of the bare Ag NCs overlap at low potential, where the amount of CO is too low to detect any difference. The activity towards CO of the Ag@Al-PMOF increases at -1.1 V/ -1.2 V vs RHE, which we attribute again to the electron transfer from the MOF to the Ag NCs. However, at -1.3 V/ -1.4 V vs RHE J_{CO} decreases, which suggests that mass transport effects of CO₂ do come into play at these higher potentials.^[47]

In addition to tuning activity and selectivity, embedding the NCs in a matrix might lead to improved stability compared with the bare NCs.^[51] To verify if the Ag NCs are stabilized by Al-PMOF in our hybrid catalyst, we performed TEM, SEM and XPS analysis of the catalysts along with ICP-OES (inductively coupled plasma - optical emission spectrometry) of the electrolyte after CO₂ electrolysis. The bare Ag NCs undergo very pronounced sintering during the CO₂RR and show dendrite formation (Figures 6a and S17a) as previously reported for Au NCs.^[58] On the other hand, sintering is strongly inhibited in the Ag@Al-PMOF (Figures 6b-d and S17b-d). In fact, the Ag NCs in the hybrids are very stable at -0.9 V vs RHE (Figures 6b and S17b). At higher potentials, the degree of sintering of NCs increases (Figure 6c,d) and they also migrate to the top of the MOF layer (Figure S17c,d); however, a high number of small NCs is still observed. Neither silver nor aluminum were detected in the electrolyte by ICP-OES after 75 min CA, confirming that the hybrids do not dissolve during this

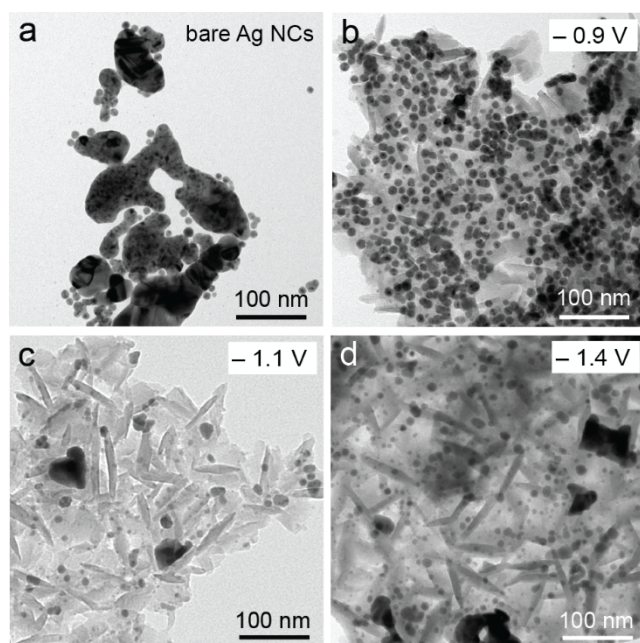


Figure 6. TEM images after 75 min of CO₂ electrolysis of (a) Ag NCs measured at -1.1 V vs RHE, (b) Ag@Al-PMOF at -0.9 V, (c) Ag@Al-PMOF at -1.1 V and (d) Ag@Al-PMOF at -1.4 V vs RHE.

time. XPS confirms the compositional stability of the Ag@Al-PMOF during electrolysis (Figure S18). Recyclability experiments (six cycles of 75 min CA at -1.1 V vs RHE) were performed (Figure S19) to determine the average turnover frequency (49 h^{-1}) and turnover number (319). Despite the overestimation of the electrocatalytic active sites, as all the Ag surface atoms were considered active, the values are comparable to those reported for CO₂RR molecular electrocatalysts immobilized in MOFs.^[14,15] The long term stability of Ag@Al-PMOF was tested by performing one continuous CA experiment for 12 h at -1.1 V vs RHE (Figure S20). However, a drop of performance was observed after the first 75-90 minutes. SEM imaging showed that in some areas the MOF layer was completely detached from the electrode and a high number of large, sintered Ag NCs was observed. On the other hand, the MOF layer appeared intact, a large ratio of the spherical Ag NCs was still retained and the current density changed less rapidly during 12 h of electrolysis at -0.9 V vs RHE (Figure S21), thus revealing increased stability of the Ag NCs embedded in the MOF at lower potentials.

Finally, to test the generality of our synthesis approach towards electrochemically active NC/MOF hybrids, we used other colloidal transition-metal NCs to synthesize hybrids with the Al-PMOF. Accordingly, Cu nanocubes (44.0 ± 5.9 nm), Au nanorods (length: 113.9 ± 9.0 nm, diameter: 39.1 ± 4.1 nm) and Au nanospheres (11.1 ± 1.0 nm) were prepared and characterized by TEM (Figure 7a-c). To synthesize the NC@MOF hybrids, the same approach previously discussed was applied for the different NCs on TEM grids (Figure 7d-f) and glassy carbon plates (Figure S22). The TEM images of the resulting hybrid structures in Figures 7d-f confirm the uniform growth of the plate-like MOF crystallites

around the different NCs. The size and shape of all of the NCs were mostly retained during the hybrid synthesis. However, the Cu nanocubes partially dissolved and lost the well-defined cubic morphology when the MOF synthesis was performed at 140 °C (Figure S23), probably due to the lower reduction potential of Cu.^[59] To mitigate the observed degradation of the Cu NCs, the temperature of the solvothermal reaction was decreased from 140 °C to 90 °C whilst keeping the other reaction parameters constant. The TEM image in Figure 7d illustrates that the Al-PMOF crystallites are still formed at the lower reaction temperature and only slight deformation of the nanocube edges was observed. The top-down SEM images in Figure S22 evidence the full coverage of the NCs by the MOF matrix. To demonstrate that all of the hybrids are electrocatalytically active, LSV was performed (Figure 7g-i). The three samples showed a higher current density in the presence of CO₂ in the electrolyte, indicating CO₂RR activity in all hybrids. Future experiments will be conducted to carefully assess the resulting product distribution and stability related to each hybrid system.

These results clearly demonstrate that the synthesis can be applied to the formation of hybrids with other metallic NCs and hence represents a new tool for the preparation of composite catalysts for the CO₂RR and eventually other electrochemical reactions. Furthermore, considering that these hybrids can be grown on different substrates, experiments to achieve higher current density could be performed by synthesizing them on carbon paper, as demonstrated in our previous work,^[60] for use in gas-diffusion electrodes.

Conclusions

In summary, we have synthesized NC@Al-PMOF hybrids which, being electrically connected to a conductive substrate, serve as model catalysts to explore how the synergistic interaction between NCs and MOFs influences electrochemical reactions, herein CO₂RR. Among these, a detailed study was conducted on the Ag@Al-PMOF hybrids. Compared to the bare Ag NCs, the hybrids drastically suppress HER, whilst promoting CO production, and also display improved structural stability compared with the bare Ag NC counterparts. The intimate contact at the interface, brought about by the removal of the native ligands, was identified as the key parameter enabling electron transfer from the Al-PMOF to the Ag NCs. We conclude electronic effects to be the main cause of the improved selectivity towards CO₂RR versus HER, together with a minor contribution of mass transport effects imposed by the porous MOF layer under the chosen testing conditions.

Going a step further from this first proof of concept, one can now think about increasing the complexity of these hybrids via mixing of organic linkers and/or secondary building units (SBUs) in the MOF^[9,61] or by metalating the porphyrin linkers.^[14,15] The addition of a redox-active metal ion will serve the double purpose of increasing the conductivity of the MOF by redox hopping,^[62-64] and to enable new catalytic synergies based, for example, on tandem catalysis (i.e. see Kornienko et al. who demonstrated that

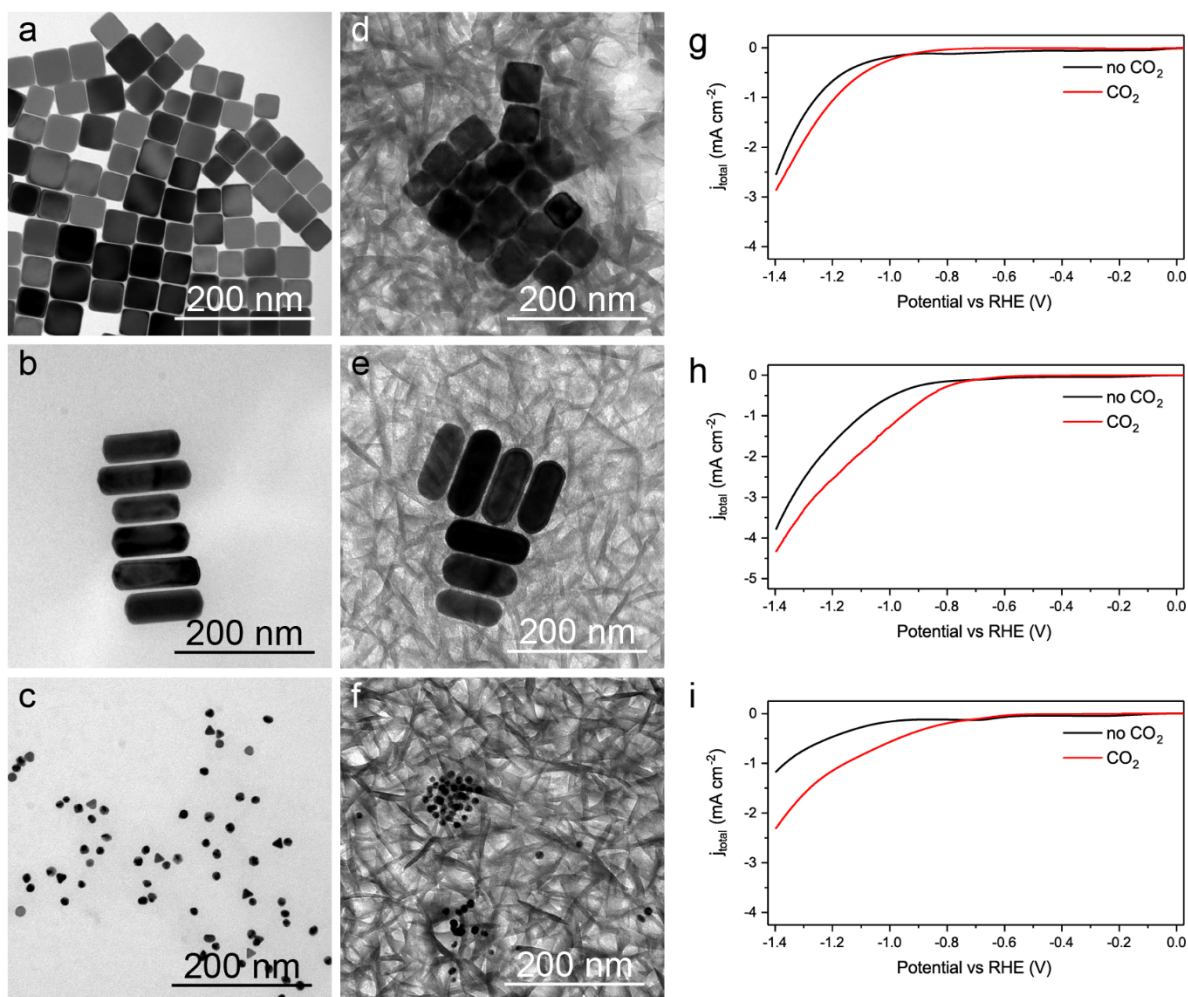


Figure 7. TEM images of (a) Cu nanocubes, (b) Au nanorods and (c) Au nanospheres and corresponding hybrids (d) Cu@Al-PMOF, (e) Au_{nanorods}@Al-PMOF and (f) Au_{nanospheres}@Al-PMOF. LSV traces of (g) Cu@Al-PMOF, (h) Au_{nanorods}@Al-PMOF and (i) Au_{nanospheres}@Al-PMOF without (black) and with CO₂ (red) in the electrolyte at a scan rate of 10 mV/sec.

Co-metalated Al-PMOF is highly selective for CO₂^[14] or on photo-driven chemistry.^[7,19]

Acknowledgements

This work was primarily supported by the European Research Council under Starting Grant ERC-HYCAT with agreement number 715634. The authors thank Dr. E. Oveisi for help with the cross-section SEM images, V. Niemann for providing the Au NC samples, Dr. A. Loiudice and S. Saris for help with the optical measurements and Dr. M. Strach for help with the GIXRD experiments. Dr. G. L. De Gregorio is acknowledged for the HPLC measurements. We thank Dr. L. F. Villalobos and Prof. K. V. Agrawal for their help with the attempted gas permeation measurements across the MOF membrane. The GIXRD experiments were performed on the Swiss-Norwegian beamline BM01 at the European Synchrotron Radiation Facility (ESRF), Grenoble, France (proposal number: 01-02 1192). We also thank

Dr. D. Chernyshov at the ESRF for providing great assistance in using beamline BM01.

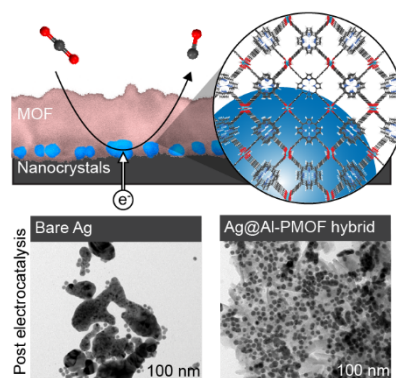
Keywords: nanoparticles, metal-organic frameworks, catalysis, CO₂ reduction, electrochemistry

- [1] J. H. Montoya, L. C. Seitz, P. Chakthranont, A. Vojvodic, T. F. Jaramillo, J. K. Nørskov, *Nat. Mater.* **2016**, *16*, 70–81.
- [2] Z. W. Seh, J. Kibsgaard, C. F. Dickens, I. Chorkendorff, J. K. Nørskov, T. F. Jaramillo, *Science* **2017**, *355*, eaad4998.
- [3] G. O. Larrazábal, A. J. Martín, J. Pérez-Ramírez, *J. Phys. Chem. Lett.* **2017**, *8*, 3933–3944.
- [4] A. Peterson, J. Nørskov, *J. Phys. Chem. Lett.* **2012**, *3*, 251–258.
- [5] H. A. Hansen, J. B. Varley, A. A. Peterson, J. K. Nørskov, *J. Phys. Chem. Lett.* **2013**, *4*, 388–392.
- [6] X. Liu, J. Xiao, H. Peng, X. Hong, K. Chan, J. K. Nørskov, *Nat. Commun.* **2017**, *1*–7.
- [7] C. S. Diercks, Y. Liu, K. E. Cordova, O. M. Yaghi, *Nat. Mater.* **2018**, *17*, 301–307.
- [8] M. B. Solomon, T. L. Church, D. M. D'Alessandro, *CrystEngComm* **2017**, *19*, 4049–4065.

- [9] S. Dou, J. Song, S. Xi, Y. Du, J. Wangm, Z.-F. Huang, Z. J. Xu, X. Wang, *Angew. Chem. Int. Ed.* **2019**, *58*, 4041–4045.
- [10] C. Zhao, X. Dai, T. Yao, W. Chen, X. Wang, J. Wang, J. Yang, S. Wei, Y. Wu, Y. Li, *J. Am. Chem. Soc.* **2017**, *139*, 8078–8081.
- [11] J. Albo, D. Vallejo, G. Beobide, O. Castillo, P. Castaño, A. Irabien, *ChemSusChem* **2017**, *10*, DOI 10.1002/cssc.201600693.
- [12] L. Ye, J. Liu, Y. Gao, C. Gong, M. Addicoat, T. Heine, C. Wöll, L. Sun, *J. Mater. Chem. A* **2016**, 2333–2345.
- [13] X. Kang, Q. Zhu, X. Sun, J. Hu, J. Zhang, Z. Liu, B. Han, *Chem. Sci.* **2016**, *7*, 266–273.
- [14] N. Kornienko, Y. Zhao, C. S. Kley, C. Zhu, D. Kim, S. Lin, C. J. Chang, O. M. Yaghi, P. Yang, *J. Am. Chem. Soc.* **2015**, *137*, 14129–14135.
- [15] I. Hod, M. D. Sampson, P. Deria, C. P. Kubiak, O. K. Farha, J. T. Hupp, *ACS Catal.* **2015**, *5*, 6302–6309.
- [16] C. W. Kung, C. O. Audu, A. W. Peters, H. Noh, O. K. Farha, J. T. Hupp, *ACS Energy Lett.* **2017**, *2*, 2394–2401.
- [17] P. De Luna, W. Liang, A. Mallick, O. Shekha, F. P. García De Arquer, A. H. Proppe, P. Todorović, S. O. Kelley, E. H. Sargent, M. Eddaoudi, *ACS Appl. Mater. Interfaces* **2018**, *10*, 31225–31232.
- [18] Y. Z. Chen, Z. U. Wang, H. Wang, J. Lu, S. H. Yu, H. L. Jiang, *J. Am. Chem. Soc.* **2017**, *139*, 2035–2044.
- [19] K. M. Choi, D. Kim, B. Rungtaweivoranit, C. A. Trickett, J. T. D. Barmanbek, A. S. Alshammari, P. Yang, O. M. Yaghi, *J. Am. Chem. Soc.* **2017**, *139*, 356–362.
- [20] A. Dhakshinamoorthy, A. M. Asiri, H. Garcia, *ACS Catal.* **2017**, *7*, 2896–2919.
- [21] M. Zhao, K. Yuan, Y. Wang, G. Li, J. Guo, L. Gu, W. Hu, H. Zhao, Z. Tang, *Nature* **2016**, *539*, 76–80.
- [22] B. Rungtaweivoranit, J. Baek, J. R. Araujo, B. S. Archanjo, K. M. Choi, O. M. Yaghi, G. A. Somorjai, *Nano Lett.* **2016**, *16*, 7645–7649.
- [23] Z. Li, R. Yu, J. Huang, Y. Shi, D. Zhang, X. Zhong, D. Wang, Y. Wu, Y. Li, *Nat. Commun.* **2015**, *6*, 8248.
- [24] K. M. Choi, K. Na, G. A. Somorjai, O. M. Yaghi, *J. Am. Chem. Soc.* **2015**, *137*, 7810–7816.
- [25] C. Rösler, R. A. Fischer, *CrystEngComm* **2015**, *17*, 199–217.
- [26] X. H. Liu, J. G. Ma, Z. Niu, G. M. Yang, P. Cheng, *Angew. Chem. Int. Ed.* **2015**, *54*, 988–991.
- [27] Y. Z. Chen, Y. X. Zhou, H. Wang, J. Lu, T. Uchida, Q. Xu, S. H. Yu, H. L. Jiang, *ACS Catal.* **2015**, *5*, 2062–2069.
- [28] G. Lu, S. Li, Z. Guo, O. K. Farha, B. G. Hauser, X. Qi, Y. Wang, X. Wang, S. Han, X. Liu, J. S. DuChene, H. Zhang, Q. Zhang, X. Chen, J. Ma, S. C. J. Loo, W. D. Wei, Y. Yang, J. T. Hupp, F. Huo, *Nat. Chem.* **2012**, *4*, 310–316.
- [29] A. Fateeva, P. A. Chater, C. P. Ireland, A. A. Tahir, Y. Z. Khimyak, P. V. Wiper, J. R. Darwent, M. J. Rosseinsky, *Angew. Chem. Int. Ed.* **2012**, *51*, 7440–7444.
- [30] N. Hoshi, M. Kato, Y. Hori, *J. Electroanal. Chem.* **1997**, *440*, 283–286.
- [31] A. Seifitokaldani, C. M. Gabardo, T. Burdyny, C.-T. Dinh, J. P. Edwards, M. G. Kibria, O. S. Bushuyev, S. O. Kelley, D. Sinton, E. H. Sargent, *J. Am. Chem. Soc.* **2018**, *140*, 3833–3837.
- [32] T. Hatsukade, K. P. Kuhl, E. R. Cave, D. N. Abram, T. F. Jaramillo, *Phys. Chem. Chem. Phys.* **2014**, *16*, 13814–13819.
- [33] B. A. Rosen, A. Salehi-khojin, M. R. Thorson, W. Zhu, D. T. Whipple, P. J. A. Kenis, R. I. Masel, *Science* **2011**, *334*, 643–645.
- [34] D. Bohra, I. Ledezma-Yanez, G. Li, W. de Jong, E. A. Pidko, W. A. Smith, *Angew. Chem. Int. Ed.* **2019**, *58*, 1345–1349.
- [35] A. Z. Weber, M. Head-Gordon, J. D. Goodpaster, A. T. Bell, M. R. Singh, *Proc. Natl. Acad. Sci.* **2017**, *114*, E8812–E8821.
- [36] S. Liu, H. Tao, L. Zeng, Q. Liu, Z. Xu, Q. Liu, J. L. Luo, *J. Am. Chem. Soc.* **2017**, *139*, 2160–2163.
- [37] A. Salehi-Khojin, H. R. M. Jhong, B. A. Rosen, W. Zhu, S. Ma, P. J. A. Kenis, R. I. Masel, *J. Phys. Chem. C* **2013**, *117*, 1627–1632.
- [38] Y. Zhao, N. Kornienko, Z. Liu, C. Zhu, S. Asahina, T. R. Kuo, W. Bao, C. Xie, A. Hexemer, O. Terasaki, P. Yang, O. M. Yaghi, *J. Am. Chem. Soc.* **2015**, *137*, 2199–2202.
- [39] S. Peng, J. M. McMahon, G. C. Schatz, S. K. Gray, Y. Sun, *Proc. Natl. Acad. Sci.* **2010**, *107*, 14530–14534.
- [40] C. Kim, T. Eom, M. S. Jee, H. Jung, H. Kim, B. K. Min, Y. J. Hwang, *ACS Catal.* **2017**, *7*, 779–785.
- [41] S. Mourdikoudis, L. M. Liz-Marzán, *Chem. Mater.* **2013**, *25*, 1465.
- [42] P. Lobaccaro, M. R. Singh, E. L. Clark, Y. Kwon, A. T. Bell, J. W. Ager, *Phys. Chem. Chem. Phys.* **2016**, *18*, 26777–26785.
- [43] T. Burdyny, W. A. Smith, *Energy Environ. Sci.* **2019**, DOI 10.1039/c8ee03134g.
- [44] A. S. Hall, Y. Yoon, A. Wuttig, Y. Surendranath, *J. Am. Chem. Soc.* **2015**, *137*, 14834–14837.
- [45] Y. Yoon, A. S. Hall, Y. Surendranath, *Angew. Chem. Int. Ed.* **2016**, *55*, 15282–15286.
- [46] M. Ma, K. Djanashvili, W. A. Smith, *Angew. Chem. Int. Ed.* **2016**, *55*, 6680–6684.
- [47] K. Yang, R. Kas, W. A. Smith, *ChemRxiv. Prepr.* **2019**, DOI 10.26434/chemrxiv.7770338.v1.
- [48] A. Dutta, M. Rahaman, M. Mohos, A. Zanetti, P. Broekmann, *ACS Catal.* **2017**, *7*, 5431–5437.
- [49] S. Huang, M. Dakhchoune, W. Luo, E. Oveisi, G. He, M. Rezaei, J. Zhao, D. T. L. Alexander, A. Züttel, M. S. Strano, K. V. Agrawal, *Nat. Commun.* **2018**, *9*, 2362.
- [50] G. Li, H. Kobayashi, J. M. Taylor, R. Ikeda, Y. Kubota, K. Kato, M. Takata, T. Yamamoto, S. Toh, S. Matsumura, H. Kitagawa, *Nat. Mater.* **2014**, *13*, 802–806.
- [51] Q. Yang, Q. Xu, H. L. Jiang, *Chem. Soc. Rev.* **2017**, *46*, 4774–4808.
- [52] J. Huang, M. Mensi, E. Oveisi, V. Mantella, R. Buonsanti, *J. Am. Chem. Soc.* **2019**, *141*, 2490–2499.
- [53] R. J. Chimentão, I. Cota, A. Dafinov, F. Medina, J. E. Sueiras, J. L. G. de la Fuente, J. L. G. Fierro, Y. Cesteros, P. Salagre, *J. Mater. Res.* **2006**, *21*, 105–111.
- [54] C. M. Gabardo, A. Seifitokaldani, J. P. Edwards, C. Dinh, T. Burdyny, G. Kibria, C. P. O. Brien, E. H. Sargent, *Energy Environ. Sci.* **2018**, *11*, 2531–2539.
- [55] Z. Cao, D. Kim, D. Hong, Y. Yu, J. Xu, S. Lin, X. Wen, E. M. Nichols, K. Jeong, J. A. Reimer, P. Yang, C. J. A. Chang, *J. Am. Chem. Soc.* **2016**, *138*, 8120–8125.
- [56] Y. J. Hwang, H. Kim, C. Kim, H. S. Jeon, C. M. Friend, T. Eom, B. K. Min, M. S. Jee, *J. Am. Chem. Soc.* **2015**, *137*, 13844–13850.
- [57] Y. C. Hsieh, S. D. Senanayake, Y. Zhang, W. Xu, D. E. Polyansky, *ACS Catal.* **2015**, *5*, 5349–5356.
- [58] K. Manthiram, Y. Surendranath, A. P. Alivisatos, *J. Am. Chem. Soc.* **2014**, *136*, 7237–7240.
- [59] A. J. Bard, L. R. Faulkner, *Electrochemical Methods - Fundamentals and Applications*, John Wiley & Sons, New York, **2001**, p. 808.
- [60] I. Luz, A. Loiudice, D. T. Sun, W. L. Queen, R. Buonsanti, *Chem. Mater.* **2016**, *28*, 3839–3849.
- [61] H. Furukawa, U. Müller, O. M. Yaghi, *Angew. Chem. Int. Ed.* **2015**, *54*, 3417–3430.
- [62] S. R. Ahrenholtz, C. C. Epley, A. J. Morris, *J. Am. Chem. Soc.* **2014**, *136*, 2464–2472.
- [63] L. Sun, M. G. Campbell, M. Dincă, *Angew. Chem. Int. Ed.* **2016**, *55*, 3566–3579.
- [64] S. Lin, P. M. Usov, A. J. Morris, *Chem. Commun.* **2018**, *54*, 6965–6974.

RESEARCH ARTICLE

Tuning reactivity through interfaces and porosity: Metal-organic framework /nanocrystals hybrids promote CO₂ reduction, suppress hydrogen evolution and improve stability. Synthetic design was key to explore these multicomponent electrocatalysts.



Yannick T. Guntern, James R. Pankhurst, Jan Vávra, Mounir Mensi, Valeria Mantella, Pascal Schouwink, and Raffaella Buonsanti*

Page No. – Page No.

Nanocrystal/Metal-Organic Framework Hybrids as Electrocatalytic Platforms for CO₂ Conversion